Galadanchi *et al.*
Natural Products and Bioprospecting (2026) 16:30
https://doi.org/10.1007/s13659-025-00581-0

Natural Products and Bioprospecting

ORIGINAL ARTICLE Open Access

Three new 14-noreudesmane-type sesquiterpenoids from the roots of *Hippophae rhamnoides*

Fatima Abdurrahman Galadanchi[1,2,3], Polina Lopukhina[1,2,3], Sisi Bai[1,2,3], Guohao Dong[1,2,3], Zhongyu Zhou[1,2,3*], Haihui Xie[1,2,3] and Xiaoyi Wei[1,2,3]

Abstract

Hippophae rhamnoides L. (Elaeagnaceae), commonly known as sea buckthorn, is a medicinal plant valued for its diverse bioactive constituents and broad therapeutic potential. Phytochemical investigation of its roots led to the isolation of three new 14-noreudesmane-type sesquiterpenoids (**1**–**3**), together with sixteen known compounds (**4**–**19**). Their structures and absolute configurations were determined using comprehensive spectroscopic analyses and quantum chemical computations of electronic circular dichroism (ECD) spectra and ^{13}C NMR shifts. Three new sesquiterpenoids (**1**–**3**) were tested for their antioxidant, anti-inflammatory, antibacterial, and *α*-glucosidase inhibitory activities. Unfortunately, none exhibited significant activity under the tested conditions. Among the isolated known compounds, all those displaying *α*-glucosidase inhibitory and antibacterial activities are pentacyclic triterpenoids. Hippophamide (**17**) showed significant DPPH and ABTS radical-scavenging activity. These results enriched the chemical profile of *H. rhamnoides* roots.

Keywords *Hippophae rhamnoides*, 14-noreudesmane sesquiterpenoids, Bioactivity

*Correspondence:
Zhongyu Zhou
zhouzhongyu@scbg.ac.cn
Full list of author information is available at the end of the article

Springer

Graphical Abstract

1 Introduction

Hippophae rhamnoides L., commonly known as sea buckthorn, is a member of the Elaeagnaceae family and is native to several regions across Asia and Europe [1, 2]. The plant is predominantly distributed in countries such as China, Turkey, Russia, Mongolia, Tajikistan, India, Greece, Afghanistan, and various other locations [3]. *H. rhamnoides* berries has long been utilized in Chinese traditional medicine to strengthen the spleen, promote digestion, relieve coughs, dispel phlegm, and invigorate blood circulation to dissipate blood stasis [4, 5]. *H. rhamnoides* is not only used in traditional Chinese medicine but also is an actinorhizal plant, which can enter a mutualistic symbiosis with *Frankia*. Extensive phytochemical analyses of *H. rhamnoides* covered various plant organs, such as the leaves [6], fruits [7, 8], branches [9], and seeds [10], and have identified a broad spectrum of secondary metabolites, including terpenoids, alkaloids, volatile oils, flavonoids and steroids. However, chemical studies on the roots remain scarce. So far, only five flavonoids have been documented from the roots [11]. In the ongoing phytochemical research on actinorhizal plant [12, 13], a detailed phytochemical studies of *H. rhamnoides* roots led to the discovery of three new 14-noreudesmane-type sesquiterpenoids (**1**–**3**), along with sixteen known compounds (**4**–**19**). This study presents the processes of extraction and isolation, followed by an in-depth structural analysis of these sesquiterpenoids. Additionally, their biological activities were evaluated, including antioxidant, anti-inflammatory, α-glucosidase inhibitory, and antibacterial properties.

2 Results and discussion

2.1 Structural elucidation

A total of nineteen compounds were successfully isolated and elucidated from the roots of *H. rhamnoides* (Fig. S1, supplementary file), including three newly identified 14-noreudesmane-type sesquiterpenoids (**1**–**3**) (Fig. 1), and sixteen known compounds (**4**–**19**) (Fig. S2, supplementary file).

Compound **1** was obtained as a brown oil with $[\alpha]_D^{25} = -14.1$ (*c* 0.19, MeOH). Its molecular formula was established to be $C_{15}H_{22}O_2$ from its molecular ion peak at *m/z* 234.1614 in the HR-EI-MS spectrum. The ^{1}H-NMR spectrum (Table 1) displayed three methyl doublets at δ_H 1.27 (3H, d, *J*=7.0 Hz, H-15), 1.25 (3H, d, *J*=7.0 Hz,

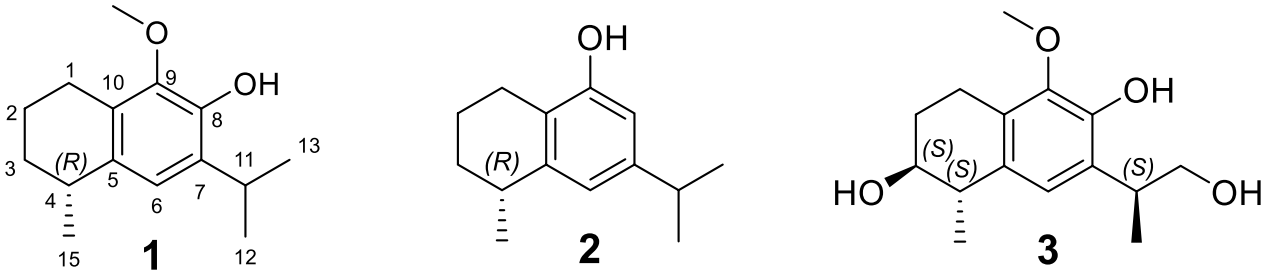

Fig. 1 The structures of compounds **1**–**3**

Table 1 ^{1}H (500 MHz) and ^{13}C (125 MHz) NMR data of compounds **1**–**3** in $CDCl_3$

	1		**2**		**3**	
No.	**δ_H, mult. (*J* in Hz)**	**δ_C**	**δ_H, mult. (*J* in Hz)**	**δ_C**	**δ_H, mult. (*J* in Hz)**	**δ_C**
1	2.71, m	23.9, CH_2	2.60, m	22.9, CH_2	2.89, m; 2.75, m	19.9, CH_2
2	1.70, m; 1.82, m	19.9, CH_2	1.89, m; 1.76, m	19.5, CH_2	2.01, dddd (13.7, 8.3, 6.0, 2.7); 1.84, m	27.3, CH_2
3	1.50, m; 1.89, m	31.5, CH_2	1.88, m; 1.54, m	30.9, CH_2	3.81, ddd (7.5, 5.5, 2.5)	72.3, CH
4	2.85, m	32.0, CH	2.89, m	32.6, CH	2.75, m	40.9, CH
5		133.9, C		143.7, C		131.5, C
6	6.84, s	121.2, CH	6.70, d (1.7)	118.7, CH	6.79, s	123.2,CH
7		132.5, C		147.3, C		128.5, C
8		143.8, C	6.52, d (1.7)	109.8, CH		145.0, C
9		143.7, C		153.1, C		144.2, C
10		127.1, C		120.3, C		126.9, C
11	3.25, m	27.4, CH	2.82, m	33.8, CH	3.30, m	36.4, CH
12	1.25, d (7.0)	22.6, CH_3	1.22, d (7.0)	24.0, CH_3	1.29, d (7.0)	16.2, CH_3
13	1.24, d (7.0)	22.6, CH_3	1.23, d (7.0)	24.1, CH_3	3.75–3.79, m	68.1, CH_2
15	1.27, d (7.0)	23.2, CH_3	1.30, d (7.1)	22.8, CH_3	1.31, d (7.0)	20.9, CH_3
OCH_3	3.78, s	60.2, CH_3			3.79, s	60.3, CH_3
Ph-OH	5.60, s		4.65, s		6.08, s	

H-12) and 1.24 (3H, d, J=7.0 Hz, H-13), as well as a singlet at δ_H 3.78, indicative of an oxygen-substituted methyl group (–OCH_3). The ^{13}C-NMR data (Table 1) in combination with the HSQC spectrum revealed a total of fifteen carbon signals, which were classified as three methyls, one oxygenated methyl, three methylenes, three methines, and five quaternary carbons. The ^{1}H-^{1}H COSY spectrum of **1** showed two spin-coupled systems of H-1/H-2/H-3/H-4/H-15 and H-12/H-11/H-13 suggesting the presence of a connections of C-1/C-2/C-3/C-4/C-15 and an isopropyl group [14] (Fig. 2). The remaining carbon signals could be ascribed to a benzene ring and an oxygenated methyl. In the HMBC spectrum, δ_H 3.25 (H-11), 1.25 (H-12), and 1.24 (H-13) correlated with δ_C 132.5 (C-7), and δ_H 3.25 (H-11) correlated with δ_C 121.2 (C-6) and 143.8 (C-8), suggesting the isopropyl group linked with the benzene ring via C-7. The HMBCs from H-1 to C-5, C-9 and C-10, from H-15 to C-5, from H-6 to C-4, indicated that the moiety of C-1/C-2/C-3/C-4/C-15 were attached to the benzene ring through C-1 linking with C-10, and through C-4 linking with C-5. To meet the requirements of the molecular formula and the presence of five quaternary carbons, a hydroxyl group should be substituted on the benzene ring. The hydroxyl group (δ_H 5.60, s) was assigned to C-8 based on its HMBC correlation to C-7. Consequently, the oxygenated methyl group

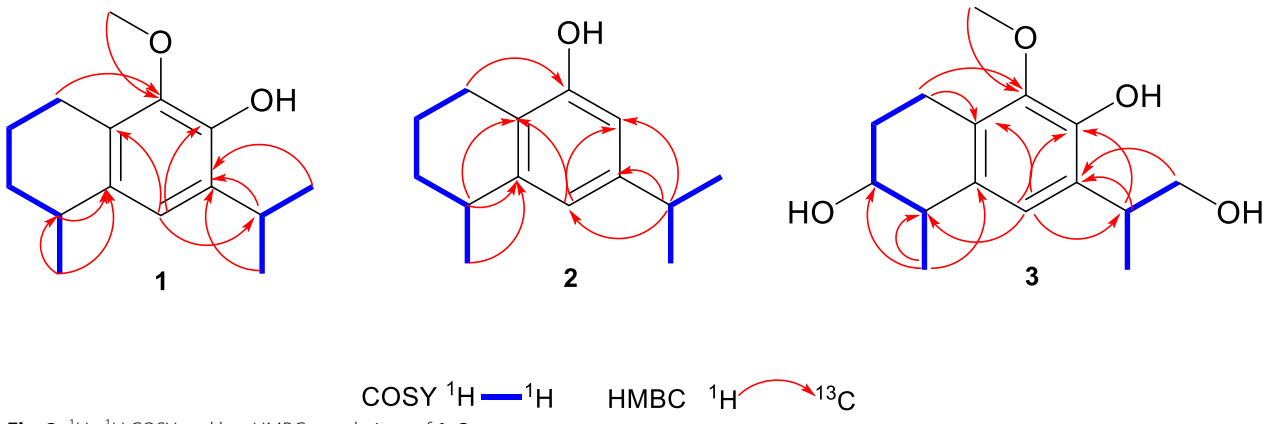

Fig. 2 ^{1}H– ^{1}H COSY and key HMBC correlations of **1–3**

was positioned at C-9. By comparing the measured electronic circular dichroism (ECD) spectra of **1** with the calculated 4*R*-**1** (Fig. 4), the absolute configuration of **1** was determined as 4*R*. Thus, compound **1** was elucidated as (4*R*)-9-methoxy-14-noreudesma-5,7,9-trien-8-ol.

Compound **2** was obtained as a pale-brown oil with $[\alpha]_D^{25} = -20$ (*c* 0.11, MeOH). It was found to have the molecular formula $C_{14}H_{20}O$ according to the molecular ion peak at *m/z* 204.1511 in the HR-EI-MS spectrum. The ^{1}H-NMR spectrum (Table 1) displayed three methyl doublets at δ_H 1.30 (3H, d, *J* = 7.1 Hz, H-15), 1.23 (3H, d, *J* = 7.0 Hz, H-13), and 1.22 (3H, d, *J* = 7.0 Hz, H-12). The ^{13}C-NMR data in combination with the HSQC spectrum revealed a total of fourteen carbon signals, which were classified into three methyls, three methylenes, four methines, and four quaternary carbons (Table 1). Its ^{1}H and ^{13}C NMR as well as ^{1}H-^{1}H COSY pattern was closely similar to that of compound **1**, which indicated that compound **2** possessed the 14-noreudesmane skeleton. The key difference between them was the absence of the methoxy group and the presence of an additional aromatic proton signal at δ_H 6.52 (1H, d, *J* = 1.7 Hz, H-8) in the ^{1}H-NMR spectrum of **2**. The coupling constant between two aromatic protons was 1.7 Hz, which indicated that they are *meta*-position. This is also confirmed by HMBCs from H-11 to C-6, C-7 and C-8. To meet the requirements of the molecular formula and the presence of four quaternary carbons, a hydroxyl group should be substituted on the benzene ring at C-9. The absolute configuration of **2** was further determined as 4*R*-2 by comparing the calculated ECD curve with its experimental values (Fig. 4). As a result, compound **2**, was fully characterized as (4*R*)-14-noreudesma-5,7,9-trien-9-ol.

Compound **3** was obtained as a brown oil with $[\alpha]_D^{25} = -12.4$ (*c* 0.15, MeOH). Its molecular formula was determined as $C_{15}H_{22}O_4$ based on the pseudo-molecular ion at *m/z* 267.1597 $[M+H]^+$ observed in positive HR-ESI–MS. The ^{1}H-NMR spectrum (Table 1) revealed resonances for one aromatic proton at δ_H 6.79 (s, H-6), two methyls at δ_H 1.29 (d, 7.0 Hz, H-12) and 1.31 (d, 7.0 Hz, H-15), and a methoxy group at δ_H 3.79 (s). The ^{13}C-NMR spectrum (Table 1) displayed fifteen carbon signals, five of which are quaternary carbons δ_C (145.0, 144.2, 131.5, 128.5, and 126.9), four methines, three methylenes, and three methyl carbons. After comparing the ^{1}H and ^{13}C NMR data with those of compound **1**, it was easy to find **3** also possesses 14-noreudesmane skeleton. With the help of the HSQC spectrum, all protons were correlated to their respective carbons (Table 1). The ^{1}H-^{1}H COSY spectrum showed two proton spin-coupled systems of H-1/H-2/H-3/H-4/H-15 and H-12/H-11/H-13 (Fig. 2). C-3 was substituted by a hydroxy group based on the observation of δ_H 3.80 (m, H-3) and δ_C (72.3, C-3). C-13 was also linked with a hydroxy group, which was confirmed in the same way like C-3. In the low-field region of ^{13}C NMR spectrum, **3** shared highly similar signal pattern of the benzene ring to that of compound **1**. The substitutions of a methoxy group at C-9 and of a hydroxy group at C-8 on the benzene ring were confirmed based on the HMBC observations from H-1 and the methoxy protons to C-9, as well as from H-11 to C-8, respectively. Consequently, compound **3** was identified as 9-methoxy-14-noreudesma-5,7,9-triene-3, 8, 13-triol. In order to assign the relative configuration of **3**, four stereoisomers, (3*S*, 4*S*, 11*R*)-, (3*R*, 4*S*, 11*R*)-, (3*S*, 4*S*, 11*S*)-, and (3*R*, 4*S*, 11*S*)-**3** were subjected to theoretical simulations for ^{13}C NMR shifts using the GIAO method [15–18]. The goodness of fit among the predicted ^{13}C NMR data of four stereoisomers and the experimental data of **3** were evaluated by the modified DP4 probability (DP4+) values [19, 20]. As can be seen in Fig. 3, the calculated ^{13}C NMR shifts of (3*S*, 4*S*, 11*S*)-isomer showed the best match with the measured data of **3** (DP4+probability: 99.35%), leading assignment of the relative configurations 3*S**, 4*S**, 11*S**. Then, (3*S*, 4*S*, 11*S*)-**3** was calculated for the ECD spectrum. As can be seen in Fig. 4, the calculated ECD curve was in excellent fit with the experimental spectrum of **3**. Thus, **3** was tentatively assigned to have the absolute configurations 3*S*, 4*S*, 11*S*.

Compounds **1**–**3** were 14-noreudesmane type sesquiterpenoids. Previously, four 14-sesquiterpenoids of this type, namely hipponorterpenes A and B, 6, 9-dihydroxy-1-oxo-14-noreudesma-5,7,9-triene and 6-hydroxy-2-isopropyl-5-methoxy-8-methylnaphthalene-1,4-dione, were also reported from *H. rhamnoides*, but from its berries and juice [14, 21]. Interestingly, such sesquiterpenoids have been isolated from some other natural sources, including *Nicotiana tabacum* (Solanaceae) [22], *Alpinia oxyphylla* (Zingiberaceae) [23], the fungus *Hypoxylon rickii* [24], and the edible mushroom *Flammulina velutipes* [25].

The sixteen known compounds were identified as arjunolic acid (**4**) [26], 18H*α*,3*β*,20*β*-ursanediol (**5**) [27], 3*β*-hydroxyolean-12-en-28-al (**6**) [28], 2*α*,3*β*,19*α*,23-tetrahydroxyolean-12-en-28-oic acid (**7**) [29], erythrodiol (**8**) [30], oleanolic acid (**9**) [31], ursolic acid (**10**) [32], maslinic acid (**11**) [33], ergosterol endoperoxide (**12**) [34], stigmast-4-en-3-one (**13**) [35], *β*-sitosterol (**14**) [36], daucosterol-6'-linoleate (**15**) [37], (+)-catechin (**16**) [38], hippophamide (**17**) [39], dehydrodiconiferyl alcohol (**18**) [40], 22-*O*-(4-hydroxy-3-methoxy-cinnamy1) docosanoic acid (**19**) [41], (Fig. S2, supplementary file), by comparing their spectroscopic data with previously documented values in literature.

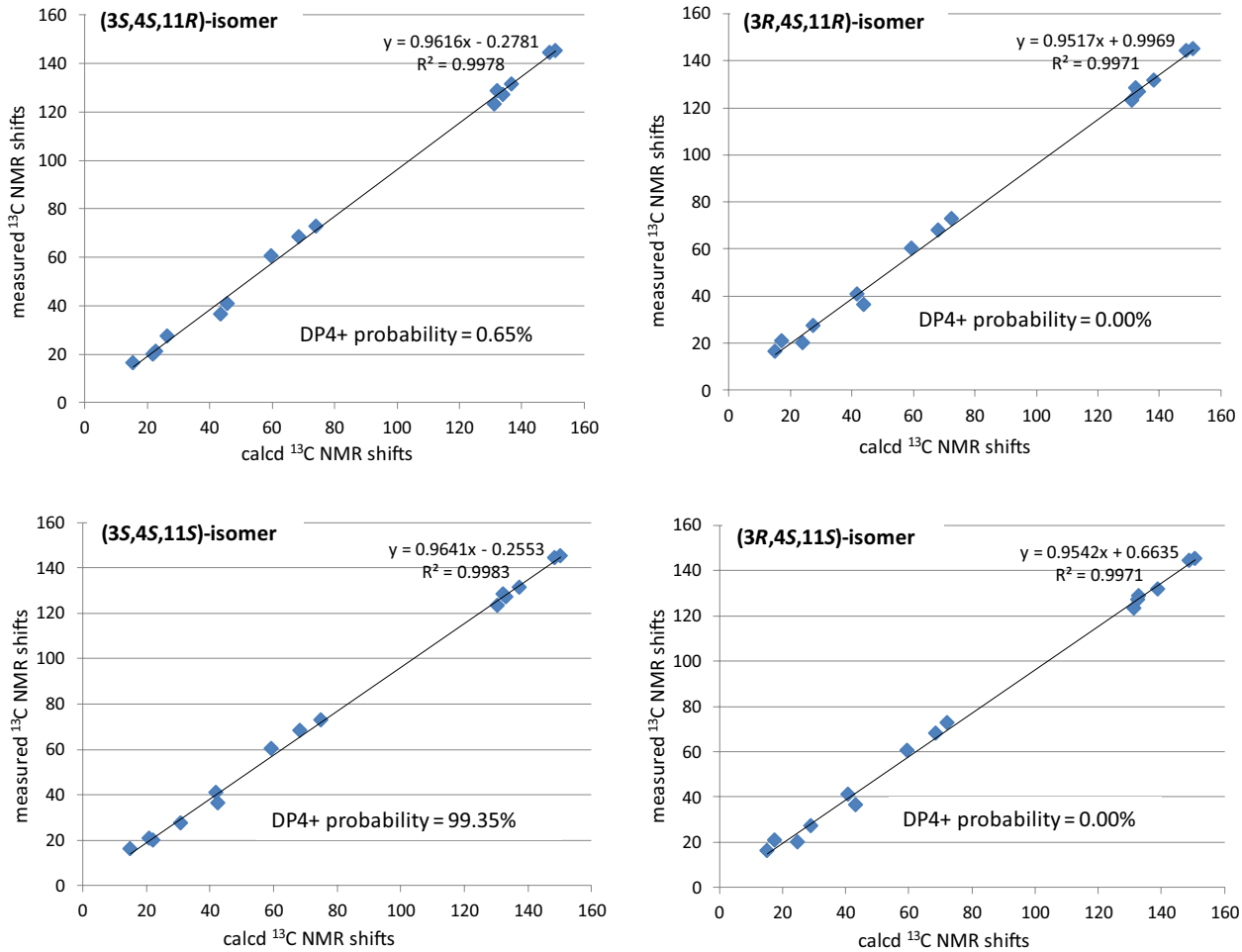

Fig. 3 Linear regression analysis of the calculated ^{13}C NMR shifts of four possible stereoisomers against the measured shifts of **3** and the goodness of fit test by DP4 + probability analysis

2.2 Antioxidant activity

The antioxidant activity of all compounds was evaluated using two in vitro assays. As summarized in Table 2, compounds **16** and **17** showed notable activity in the DPPH radical scavenging assay, with IC_{50} values of 30.66 μM and 43.15 μM, respectively, compared to *L*-ascorbic acid (IC_{50} = 23.77 μM). In the ABTS cation radical scavenging assay, both compounds **16** and **17** displayed even stronger activity, with IC_{50} values of 13.17 μM and 20.31 μM, respectively, outperforming L-ascorbic acid (IC_{50} = 24.85 μM). Three new compounds **1**–**3** were tested in the cellular reactive oxygen species (ROS) scavenging assay at 50 μM. All of them showed inhibition rate below 10%. Compared to curcumin (IC_{50} = 16.84 μM), the intracellular antioxidant activity of these compounds was negligible.

2.3 *α*-Glucosidase inhibitory activity

Compounds **1**–**19** were evaluated for their inhibitory activity against *α*-glucosidase, using corosolic acid as positive control. As shown in Table 3, compound **10** exhibited the most potent inhibitory effect, with an IC_{50} value of 4.81 *μ*M, equivalent to that of corosolic acid (IC_{50} = 5.60 *μ*M). Compounds **4**, **5**, **8**, **9**, and **11** showed moderate activity, with IC_{50} values ranging from 8.96 to 33.58 *μ*M. All active compounds are triterpenoids, while the positive control corosolic acid is also a triterpenoid.

2.4 Antibacterial activity

All 19 isolated compounds were evaluated for their antibacterial activity against three bacterial strains: *Staphylococcus aureus* (MSSA, CMCC 26003), methicillin-resistant *Staphylococcus aureus* (MRSA, JCSC 3063), and *Escherichia coli* (EC, ATCC 8739) (Table 4). Minimum inhibitory concentrations (MICs) were determined and compared with positive controls, including

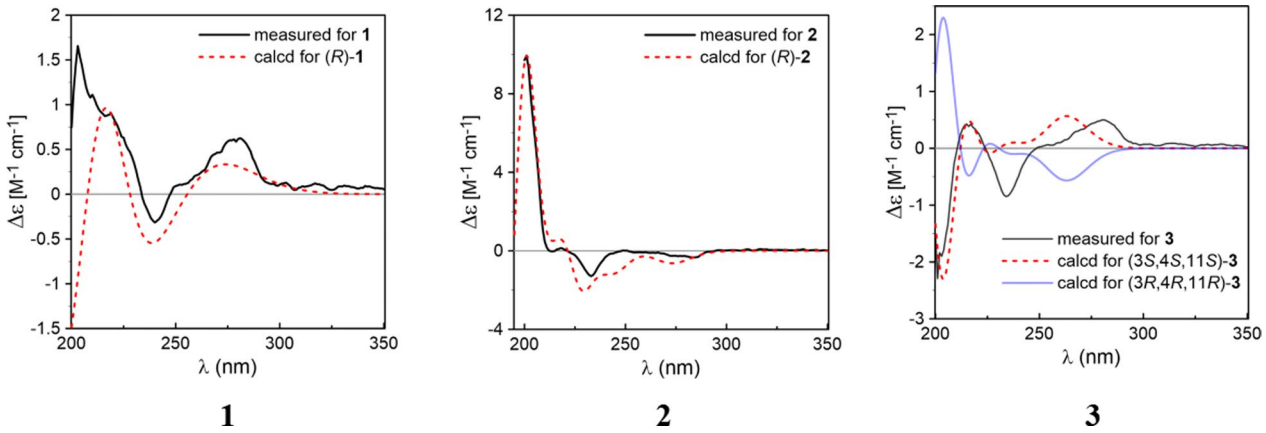

Fig. 4 Comparison of the measured and calculated ECD spectra of **1–3** in methanol

kanamycin, vancomycin, and polymyxin. Among the tested compounds, compound **9** exhibited weak antibacterial activity against MSSA and MRSA, with an MIC of 100 μM. Compound **10** displayed weak antibacterial activity against both MSSA and MRSA, with an MIC value of 25 μM. None of the compounds demonstrated antibacterial activity against the Gram-negative strain *E. coli*.

2.5 Anti-inflammatory activity

To evaluate the anti-inflammatory potential of three new compounds (**1–3**), their ability to suppress nitric oxide (NO) production was tested using LPS-stimulated RAW 264.7 murine macrophage cells. Compounds **1–3** were tested at concentrations of 50, 25 and 10 μM. However, these compounds exhibited NO production inhibitory rates below 10% at all concentrations tested, compared to the positive control, indomethacin (IC_{50} = 36.29 μM).

Table 2 Antioxidant activity of compounds **1–19**

Compounds	DPPH (IC_{50}, μM)	ABTS (IC_{50}, μM)	Cellular ROS (% inhibition rate)
1	> 50	> 50	4.38 ± 2.83[c]
2	> 50	> 50	−12.79 ± 4.48[c]
3	> 50	> 50	3.17 ± 3.04[c]
4–15	> 50	> 50	NT[b]
16	30.66 ± 0.64	13.17 ± 0.13	NT[b]
17	43.15 ± 0.89	20.31 ± 0.53	NT[b]
18–19	> 50	> 50	NT[b]
L-Ascorbic acid[a]	23.77 ± 1.02	24.85 ± 1.17	NT[b]
Curcumin[a]	NT[b]	NT[b]	16.84 ± 0.28 μM

Values are Mean ± SD (n = 3)

[a] Positive control

[b] *NT* Not tested

[c] Tested at 50 μM

3 Experimental procedures

3.1 General

Column chromatography (CC) was performed using silica gel (80–100 mesh and 200–300 mesh; Yantai Jiangyou Silica Gel Development Co., Ltd., Yantai, China), Sephadex LH-20 (Pharmacia Fine Chemicals Co., Ltd., Uppsala, Sweden), and reversed-phase C_{18} (YMC Co., Ltd., Japan) materials. Preparative high-performance liquid chromatography (HPLC) was carried out with an LC-6AD pump system equipped with an SPD UV/Vis detector (Shimadzu, Kyoto, Japan), using a Cosmosil column (250 mm × 10 mm i.d., 5 μm

Table 3 α-Glucosidase inhibitory activity of compounds **1–19**

Compounds	IC_{50} (μM)	Compound	IC_{50} (μM)
1–3	> 50	**9**	10.16 ± 0.38
4	33.58 ± 1.69	**10**	4.81 ± 0.28
5	30.14 ± 2.00	**11**	11.80 ± 1.49
6–7	> 50	**12–19**	> 50
8	8.96 ± 0.40	Corosolic acid[a]	5.60 ± 0.24

Values are Mean ± SD (n = 3)

[a] Positive control

Table 4 Antibacterial activity of compounds **1–19** (MIC, μM)

Compounds	MSSA	MRSA	EC
1–8	> 100	> 100	> 100
9	100	100	> 100
10	25	25	> 100
11–19	> 100	> 100	> 100
Kanamycin[a]	1.25	> 40	NT[b]
Vancomycin[a]	NT[b]	2.5	NT[b]
Polymyxin[a]	NT[b]	NT[b]	1.25

[a] Positive control

[b] *NT* Not tested; (n = 3)

particle size, Kyoto, Japan) at a flow rate of 2 mL/min. Thin-layer chromatography (TLC) was performed on precoated silica gel plates (HSGF254; Yantai Jiangyou Silica Gel Development Co., Ltd., Yantai, China), with spot detection achieved by spraying with a 5% vanillin in sulfuric acid solution followed by heating. Proton (^{1}H) and carbon (^{13}C) nuclear magnetic resonance (NMR) spectra were recorded on a Bruker DRX-500 NMR spectrometer (Bruker Biospin GmbH, Rheinstetten, Germany), with chemical shifts referenced to residual solvent peaks. The spectrometer operated at 500 MHz for ^{1}H NMR and 125 MHz for ^{13}C NMR. High-resolution electron impact mass spectrometry (HR-EI-MS) and Electrospray ionization mass spectrometry (ESI–MS) data were obtained using a Thermo Scientific DFS magnetic mass spectrometer (Thermo Corporation). Optical rotation values (α_D) were measured on a Perkin-Elmer 343 polarimeter using methanol (MeOH) as the solvent. Circular Dichroism (CD) spectrum was recorded on a Chirascan circular dichroism spectrometer (Applied Photophysics Ltd., Surrey, UK).

3.2 Plant material

Roots of *Hippophae rhamnoides* were collected in April 2023 from Diqing, Yunnan province, China, by Kunming Zhifen Biotechnology Company, and were botanically authenticated by this company. A voucher specimen (No. Zzy20230414) was deposited at the phytochemistry laboratory, South China Botanical Garden, Chinese Academy of Sciences.

3.3 Extraction and isolation

The air-dried roots were pulverized into a fine powder (14 kg) and extracted three times with 95% aqueous ethanol. The combined filtrates were concentrated under reduced pressure to obtain a crude extract weighing 1007.6 g. The extract was successively partitioned with petroleum ether (4.5 L × 3), ethyl acetate (4.5 L × 3), and *n*-butanol (4.5 L × 3). The resulting fractions were concentrated to dryness under vacuum yielding petroleum ether-soluble (38.0 g), ethyl acetate-soluble (75.2 g), and *n*-butanol-soluble (418.8 g) fractions. The ethyl acetate fraction (75.2 g) underwent purification through silica gel column chromatography (CC), Sephadex LH-20 CC, preparative high-performance liquid chromatography (HPLC), and reversed-phase C_{18} (RP-C_{18}) CC to isolate individual compounds. A comprehensive flowchart detailing the phytochemical extraction and isolation procedure for compounds **1–19** is provided in Fig. S2, supplementary file.

3.4 Spectroscopic data new compounds

3.4.1 (4R)-9-Methoxy-14-noreudesma-5,7,9-trien-8-ol (1)

Brown oil; $[\alpha]_D^{25} = -14.1$ (*c* 0.19, MeOH); UV (MeOH) λ_{max} nm (log ε): 202 (3.60), 280 (2.44); HR-EI-MS *m/z* 234.1614 (calculated for $C_{15}H_{22}O_2$, 234.1614); ^{1}H (500 MHz) and ^{13}C (125 MHz) NMR data, see Table 1.

3.4.2 (4R)-14-Noreudesma-5,7,9-trien-9-ol (2)

Pale brown oil; $[\alpha]_D^{25} = -20$ (*c* 0.11, MeOH); UV (MeOH) λ_{max} nm (log ε): 203 (3.63), 281 (2.35); HR-EI-MS *m/z* 204.1511 (calculated for $C_{14}H_{20}O$, 204.1509); ^{1}H (500 MHz) and ^{13}C (125 MHz) NMR data, see Table 1.

3.4.3 9-Methoxy-14-noreudesma-5,7,9-triene-3,8,13-triol (3)

Brown oil; $[\alpha]_D^{25} = -12.4$ (*c* 0.15, MeOH); UV (MeOH) λ_{max} nm (log ε): 203 (3.61), 281 (2.43); HR-ESI–MS (positive) *m/z* 267.1597 (calculated for $C_{15}H_{23}O_4$, 267.1591); ESI–MS (positive) *m/z* 267 $[M+H]^+$ and 289 $[M+Na]^+$, $C_{15}H_{22}O_4$; ^{1}H (500 MHz) and ^{13}C (125 MHz) NMR data, see Table 1.

3.5 Computational details

Conformational search was done using Molecular Merck force field (MMFF) embedded in Spartan'14 software (Wavefunction Inc., Irvine, CA, USA). Density functional theory (DFT) and time-dependent density functional theory (TDDFT) calculations were performed with Gaussian09 RevD.01 [42]. Double-hybrid (DH) DFT calculations were conducted with ORCA 5.0.4 program package using RIJCOSX approximation, tight SCF criteria [43]. For conformational analysis, conformers of compounds **1**, **2** and **3** each within an 8 kcal/mol energy window from MMFF conformational search were subjected to geometry optimizations followed by frequency calculations using DFT method at the B3LYP [44, 45] -GD3BJ [46, 47] /6-31G(d) level of theory. To simulate the ^{13}C NMR shifts of **3**, the optimized low-energy conformers (relative electronic energies < 4.0 kcal/mol) were subjected to NMR calculations using the gauge including atomic orbitals (GIAO) [15, 17, 18] method at the mPW1PW91/6–311 + G (d, p) level [16] of theory with the solvent model PCM for chloroform. The unscaled chemical shifts (δ_u) were computed using TMS as reference standard according to $\delta_u = \sigma_0 - \sigma^x$ (where σ^x is the Boltzmann averaged shielding tensor and σ_0 is the shielding tensor of TMS computed at the same level employed for σ^x). The Boltzmann averaging was done using the relative energies obtained from the single-point NMR calculations [19, 20] The goodness of fit test between the simulated ^{13}C NMR data of the four stereoisomers and the experimental shifts of **3** were evaluated by the improved DP4 probability (DP4 +) [19, 20]. For calculations of the ECD spectra, the optimized geometries were subjected to single point calculations using the DH-DFT method at the (PWPB95

[48]-GD3BJ/def2-QZVPP [49] level of theory with the SMD [50] solvent model for MeOH to obtain more accurate electronic energies. The TDDFT calculations were carried out using M06-2X [51], PBE1PBE (PBE0) [52], M11-L [53], and revTPSS [54] functionals in combination with the TZVP [51] basis set and the PCM solvation model for MeOH. The number of excited states was 30 for all conformers. The results were visualized and exported using the SpecDis program [55]. The calculated ECD spectra was generated as a sum of Gaussian curve using rotatory strengths computed in the dipole-velocity gauge from ECD data of the individual conformers. Boltzmann distributions of the conformers in equilibrium population were estimated from the relative Gibbs free energies (ΔG) at 298.15K.

3.6 Antioxidant activity

Antioxidant activity was evaluated by in vitro DPPH radical scavenging assay, ABTS radical cation scavenging assay, and cellular reactive oxygen species (ROS) scavenging assay following our lab previous methods [56, 57].

3.7 α-Glucosidase activity

The α-glucosidase inhibitory activity of compounds **1–19** was assessed based on a previously reported method with slight modifications [58]. In a 96-well microtiter plate, 70 μL of phosphate buffer, 10 μL of α-glucosidase enzyme solution (0.5 U/mL), and 10 μL of the test compound at varying concentrations (50, 25, 12.5, 6.25, and 3.12 μM) were added to each well. Corosolic acid (10 μL) was used as a positive control. For the negative control, the test compound was replaced with phosphate buffer, while the blank control was prepared by omitting the enzyme and substituting it with buffer. The reaction mixtures were incubated at 37 °C for 10 min, followed by the addition of 10 μL of PNPG solution per well. After a further 20 min incubation at 37 °C, the reaction was terminated by adding 100 μL of Na_2CO_3 solution. The absorbance was measured at 405 nm using a microplate reader. All experiments were conducted in triplicate, and results are expressed as mean values ± standard deviation (SD).

$$\text{Inhibition (\%)} = \left[1 - \frac{(OD_{sample} - OD_{blank})}{(OD_{negative} - OD_{blank})}\right] \times 100\%$$

3.8 Antibacterial activity

The antibacterial activity of compounds **1–19** was evaluated against *Staphylococcus aureus* (MSSA, CMCC 26003), methicillin-resistant *Staphylococcus aureus* (MRSA, JCSC 3063), and *Escherichia coli* (EC, ATCC 8739) using a resazurin-based microdilution assay. Bacterial suspensions were prepared by adding 30 μL of the inoculum to 5 mL of Brain Heart Infusion (BHI) medium followed by incubation at 37 °C in a shaking incubator set at 200 rpm for 12 h. The bacterial suspension was then diluted to an optical density (OD) of 0.07 ± 0.002, corresponding to 1.25×10^6 CFU/mL. A resazurin stock solution (1 mg/mL) was prepared in sterile water and diluted to 100 μg/mL for use. Stock solutions of compounds were prepared in biological-grade DMSO at 1 mM, and used as test samples. The assay was performed on 96-well plates. First, 90 μL of a resazurin-bacterial mixed solution (in a 3:2 volume ratio) and 10 μL of the test samples were added to the first row (Row A) and thoroughly mixed using a pipette. Then, 50 μL of the resazurin-bacterial solution was added to rows B–H. Next, 50 μL mixture from Row A was transferred to Row B and mixed well; this process was repeated for Rows C–H. Two-fold serial dilutions were performed across the rows. The plate was incubated at 37°C for 6–8 h. The MIC was determined by the lowest concentration at which the bacterial solution changed from purple to pink, indicating inhibition of growth. Each test was performed in triplicate. All bacterial strains were obtained from the Guangdong Institute of Microbiology (Guangzhou, China). Vancomycin and kanamycin were used as positive controls for MSSA and MRSA, and polymyxin for EC.

3.9 Anti-inflammatory activity

The anti-inflammatory potential of compounds **1–3** was evaluated by measuring their ability to inhibit nitric oxide (NO) production in lipopolysaccharide (LPS)-stimulated RAW 264.7 macrophages, following our previously established protocols [57].

4 Conclusion

In conclusion, the phytochemical exploration of *H. rhamnoides* roots yielded three new 14-noreudesmane-type sesquiterpenoids and a suite of known compounds. The main constituents were oleanane-type triterpenoids. While the newly identified sesquiterpenoids exhibited limited biological activity, several triterpenoids demonstrated promising α-glucosidase inhibitory, and antibacterial properties. Hippophamide (**17**) showed significant antioxidant activity with DPPH and ABTS

radicals scavenging potential. These results enriched the chemical profile of *H. rhamnoides* roots.

Supplementary Information

The online version contains supplementary material available at https://doi.org/10.1007/s13659-025-00581-0.

Supplementary material 1

Acknowledgements
We would like to thank Mr. Yunfei Yuan, South China Botanical Garden, Chinese Academy of Sciences (CAS), for NMR spectroscopic measurements; Dr. Hanxiang Li, South China Botanical Garden, CAS, for GC-EI-MS experiment; Prof. Ping Wu, South China Botanical Garden, Chinese Academy of Sciences, for ESI-MS experiment; Prof. Changan Geng, Kunming Institute of Botany, CAS, for EI- and HR-EI-MS experiment; Senior engineer Aijun Sun, Institute of South China Sea Oceanology, CAS, for ECD experiment. The photo of *Hippophae rhamnoides* fruits used in Graphical Abstract is courtesy of Prof. Caiyun He, Research Institute of Forestry, Chinese Academy of Forestry.

Author contributions
FAG carried out the methodology, investigation, formal analysis, visualization, data curation, writing—original draft, and writing—review & editing; PL contributed to biological investigation; SB contributed to isolation; GD contributed to isolation and formal analysis; ZZ was responsible for conceptualization, supervision, validation, resources, funding acquisition, project administration, and writing—review & editing; HX and XW contributed to ECD calculations, writing—review & editing, and project supporting. All authors read and approved the final manuscript.

Funding
This research was supported by the Natural Science Foundation of Guangdong Province (grant number 2025A1515010367), National Natural Science Foundation of China (grant number 31970376), and Guangdong Science and Technology Plan Project (grant number 2023B1212060046).

Data availability
The experimental data supporting this work are accessible within the article and its Additional file 1.

Declarations

Competing interests
The authors declare that they have no known financial or personal competing interests that could have influenced the research reported in this manuscript.

Author details
[1]Guangdong Provincial Key Laboratory of Applied Botany and Key Laboratory of National Forestry and Grassland Administration On Plant Conservation and Utilization in Southern China, South China Botanical Garden, Chinese Academy of Sciences, Guangzhou 510650, China. [2]South China National Botanical Garden, Guangzhou 510650, China. [3]University of Chinese Academy of Sciences, Beijing 100049, China.

Received: 19 October 2025 Accepted: 7 December 2025
Published online: 04 February 2026

References

1. Singh V. Global distribution of sea buckthorn (Hippophae sp) resources and their utilization. In: The Sea Buckthorn Genome. UK: Springer International Publishing; 2022.
2. Jubayer MF, Mazumder MAR, Nayik GA, Ansari MJ, Ranganathan TV. *Hippophae rhamnoides* L.: Sea buckthorn. In: Immunity Boosting Medicinal Plants of the Western Himalayas. UK: Springer; 2023.
3. Ma QG, He NX, Huang HL, Fu XM, Zhang ZL, Shu JC, et al. *Hippophae rhamnoides* L.: a comprehensive review on the botany, traditional uses, phytonutrients, health benefits, quality markers, and applications. J Agric Food Chem. 2023;71:4769–88.
4. Dong W, Tang Y, Qiao J, Dong Z, Cheng J. Sea buckthorn bioactive metabolites and their pharmacological potential in digestive diseases. Front Pharmacol. 2025;16:1637676.
5. He N, Wang Q, Huang H, Chen J, Wu G, Zhu M, et al. A comprehensive review on extraction, structure, detection, bioactivity, and metabolism of flavonoids from sea buckthorn (*Hippophae rhamnoides* L.). J Food Biochem. 2023;2023:4839124.
6. Kubczak M, Khassenova AB, Skalski B, Michlewska S, Wielanek M, Sklodowska M, et al. *Hippophae rhamnoides* L. leaf and twig extracts as rich sources of nutrients and bioactive compounds with antioxidant activity. Sci Rep. 2022;12:1095.
7. Ma Q, Guan Y, Sang Z, Dong J, Wei R. Isolation and characterization of auronlignan derivatives with hepatoprotective and hypolipidemic activities from the fruits of *Hippophae rhamnoides* L. Food Funct. 2022;13:7750–61.
8. Lee DE, Park KH, Hong JH, Kim SH, Park KM, Kim KH. Anti-osteoporosis effects of triterpenoids from the fruit of sea buckthorn (*Hippophae rhamnoides*) through the promotion of osteoblast differentiation in mesenchymal stem cells, C3H10T1/2. Arch Pharm Res. 2023;46:771–81.
9. Tkacz K, Wojdyło A, Turkiewicz IP, Nowicka P. Triterpenoids, phenolic compounds, macro-and microelements in anatomical parts of sea buckthorn (*Hippophae rhamnoides* L.) berries, branches and leaves. J Food Compos Anal. 2021;103:104107.
10. Ding J, Hu N, Li G, Wang H-L. Megastigmanes and flavonoids from seeds of *Hippophae rhamnoides*. Chem Nat Compd. 2024;60:21–5.
11. Hibasami H, Mitani A, Katsuzaki H, Imai K, Yoshioka K, Komiya T. Isolation of five types of flavonol from sea buckthorn (*Hippophae rhamnoides*) and induction of apoptosis by some of the flavonols in human promyelotic leukemia HL-60 cells. Int J Mol Med. 2005;15:805–9.
12. Xu Y, Xu Y, Huang Z, Luo Y, Gao R, Xue J, et al. 3-pentanol glycosides from root nodules of the actinorhizal plant *Alnus cremastogyne*. Phytochemistry. 2023;207:113582.
13. Jin Y, Xu Y, Huang Z, Zhou Z, Wei X. Metabolite pattern in root nodules of the actinorhizal plant *Casuarina equisetifolia*. Phytochemistry. 2021;186:112724.
14. Rédei D, Kúsz N, Rafai T, Bogdanov A, Burián K, Csorba A, et al. 14-noreudesmanes and a phenylpropane heterodimer from sea buckthorn berry inhibit Herpes simplex type 2 virus replication. Tetrahedron. 2019;75:1364–70.
15. Wolinski K, Hinton JF, Pulay P. Efficient implementation of the gauge-independent atomic orbital method for NMR chemical shift calculations. J Am Chem Soc. 1990;112:8251–60.
16. Lodewyk MW, Soldi C, Jones PB, Olmstead MM, Rita J, Shaw JT, et al. The correct structure of aquatolide-experimental validation of a theoretically predicted structural revision. J Am Chem Soc. 2012;134:18550–3.
17. Ditchfield R. Self-consistent perturbation theory of diamagnetism: I. a gauge-invariant LCAO method for NMR chemical shifts. Mol Phys. 1974;27:789–807.
18. Ditchfield R. Molecular orbital theory of magnetic shielding and magnetic susceptibility. J Chem Phys. 1972;56:5688–91.
19. Smith SG, Goodman JM. Assigning stereochemistry to single diastereoisomers by GIAO NMR calculation: the DP4 probability. J Am Chem Soc. 2010;132:12946–59.
20. Grimblat N, Zanardi MM, Sarotti AM. Beyond DP4: an improved probability for the stereochemical assignment of isomeric compounds using quantum chemical calculations of NMR shifts. J Org Chem. 2015;80:12526–34.
21. Zhang XL, Na HY, Li PS, Chen YX, Li ZL, Liang GD, et al. Hipponorterpenes A and B, two new 14-noreudesmane-type sesquiterpenoids from the juice of *Hippophae rhamnoides*. Phytochem Lett. 2022;52:82–6.
22. Yang CY, Geng CA, Huang XY, Wang H, Xu HB, Liang WJ, et al. Noreudesmane sesquiterpenoids from the leaves of *Nicotiana tabacum*. Fitoterapia. 2014;96:81–7.
23. Park DH, Lee JW, Jin Q, Jeon WK, Lee MK, Hwang BY. A new noreudesmane-type sesquiterpenoid from *Alpinia oxyphylla*. Bull Korean Chem Soc. 2014;35:1565–7.

24. Kuhnert E, Surup F, Wiebach V, Bernecker S, Stadler M. Botryane, noreudesmane and abietane terpenoids from the ascomycete *Hypoxylon rickii*. Phytochemistry. 2015;117:116–22.
25. Tao Q, Ma K, Yang Y, Wang K, Chen B, Huang Y, et al. Bioactive sesquiterpenes from the edible mushroom *Flammulina velutipes* and their biosynthetic pathway confirmed by genome analysis and chemical evidence. J Org Chem. 2016;81:9867–77.
26. Ramesh AS, Christopher JG, Radhika R, Setty CR, Thankamani V. Isolation, characterisation and cytotoxicity study of arjunolic acid from *Terminalia arjuna*. Nat Prod Res. 2012;26:1549–52.
27. Wang F, Li ZL, Cui HH, Hua HM, Jing YK, Liang SW. Two new triterpenoids from the resin of *Boswellia carterii*. J Asian Nat Prod Res. 2011;13:193–7.
28. Kamiya K, Yoshioka K, Saiki Y, Ikutat A, Satak T. Triterpenoids and flavonoids from *Paeonia lactiflora*. Phytochemistry. 1997;44:141–4.
29. Xia M, Tan J, Yang L, Shang Z, Zhao Q, Shi G. Studies on chemical constituents in *Patrinia scabiosaefolia*. Chin Tradit Herbal Drugs. 2010;41:1612–5.
30. Osman W, Ibrahim M, Adam M, Mothana R, Mohammed M, Abdoon I, et al. Isolation and characterization of four terpenoidal compounds with potential antimicrobial activity from Tarconanthus camphorantus L. (Asteraceae). J Pharm Bioallied Sci. 2019;11:373–9.
31. Castellano JM, Sara RR, Perona JS. Oleanolic acid: extraction, characterization and biological activity. Nutrients. 2022;14:623.
32. Gnoatto SC, Klimpt AD, Nascimento SD, Galera P, Boumediene K, Gosmann G, et al. Evaluation of ursolic acid isolated from *Ilex paraguariensis* and derivatives on aromatase inhibition. Eur J Med Chem. 2008;43:1865–77.
33. Murakami C, Myoga K, Kasai R, Ohtani K, Kurokawa T, Ishibashi S, et al. Screening of plant constituents for effect on glucose transport activity in *Ehrlich ascites* tumour cells. Chem Pharm Bull. 1993;41:2129–31.
34. Kwon HC, Zee SD, Cho SY, Chop SU, Lee KR. Cytotoxic ergosterols from *Paecilomyces* sp. J300. Arch Pharm Res. 2002;25:851–5.
35. Jibril S, Sirat HM, Zakari A, Sani IM, Kendeson CA, Abdullahi Z, et al. Isolation of chemical constituents from n-hexane leaf extract of *Cassia singueana* del. (Fabaceae). Chem Search J. 2019;10:14–20.
36. Ododo MM, Choudhury MK, Dekebo AH. Structure elucidation of *β*-sitosterol with antibacterial activity from the root bark of *Malva parviflora*. Springerplus. 2016;5:1–11.
37. Zhimin L, Lijun W, Bingya J, Bohang S, Huang J, Huiyuan G. Chemical constituents of chestnut kernel (III). J Shenyang Pharm Univ. 2008;25:856.
38. Zhu XD, Xu B, Wang F. Studies on the chemical components of *Osyris wightiana*. Nat Prod Res Dev. 2009;21:956–9.
39. OuYang J, Zhou WN, Li G, Wang XY, Ding CX, Suo YR, et al. Three new alkaloids from *Hippophae rhamnoides* Linn. subsp. *sinensis* Rousi. Helv Chim Acta. 2015;98:1287–91.
40. Guangshu W, Muxin Z, Xiaohong Y, Jingda X. Studies on the non-alkaloid constituents of *Hippeastrun vittatum* in Amaryllidaceae. Chin Pharm J. 2005;40:498–9.
41. Wang Yan WY, Su BingHe SB, Zhou XiaoYu ZX, Wang TianMin WT, Zhai YanJun ZY. Study on chemical constituents of processed fructus *Polygoni orientalis*. Liaoning J Tradit Chin Med. 2012;39:505–8.
42. Gaussian 09, revision D.01. 2013, Gaussian, Inc.: Wallingford CT.
43. Neese F. Software update: the ORCA program system, version 4.0. WIRES Comput Mol Sci. 2018;8:e1327.
44. Becke AD. Density-functional thermochemistry III. The role of exact exchange. J Chem Phys. 1993;98:5648–52.
45. Lee CT, Yang WT, Parr RG. Development of the Colle-Salvetti correlation-energy formula into a functional of the electron density. Phys Rev B. 1988;37:785–9.
46. Grimme S, Antony J, Ehrlich S, Krieg H. A consistent and accurate ab initio parametrization of density functional dispersion correction (DFT-D) for the 94 elements H-Pu. J Chem Phys. 2010;132:154104.
47. Grimme S, Ehrlich S, Goerigk L. Effect of the damping function in dispersion corrected density functional theory. J Comput Chem. 2011;32:1456–65.
48. Goerigk L, Grimme S. Efficient and accurate Double-Hybrid-Meta-GGA density functionals evaluation with the extended GMTKN30 database for general main group thermochemistry, kinetics, and noncovalent interactions. J Chem Theory Comput. 2011;7:291–309.
49. Weigend F, Ahlrichs R. Balanced basis sets of split valence, triple zeta valence and quadruple zeta valence quality for H to Rn: design and assessment of accuracy. Phys Chem Chem Phys. 2005;7:3297–305.
50. Marenich AV, Cramer CJ, Truhlar DG. Universal solvation model based on solute electron density and on a continuum model of the solvent defined by the bulk dielectric constant and atomic surface tensions. J Phys Chem B. 2009;113:6378–96.
51. Chen G, Wang Y, Zhao C, Korpelainen H, Li C. Genetic diversity of *Hippophae rhamnoides* populations at varying altitudes in the Wolong natural reserve of China as revealed by ISSR markers. Silvae Genet. 2008;57:29.
52. Perdew JP, Burke K, Ernzerhof M. Generalized gradient approximation made simple. Phys Rev Lett. 1996;77:3865–8.
53. Peverati R, Truhlar DG. M11-L: a local density functional that provides improved accuracy for electronic structure calculations in chemistry and physics. J Phys Chem Lett. 2012;3:117–24.
54. Perdew JP, Ruzsinszky A, Csonka GI, Constantin LA, Sun JW. Workhorse semilocal density functional for condensed matter physics and quantum chemistry. Phys Rev Lett. 2009;103:026403.
55. Bruhn T, Schaumloeffel A, Hemberger Y, Bringmann G. SpecDis: quantifying the comparison of calculated and experimental electronic circular dichroism spectra. Chirality. 2013;25:243–9.
56. Ma Q, Xie H, Li S, Zhang R, Zhang M, Wei X. Flavonoids from the pericarps of *Litchi chinensis*. J Agric Food Chem. 2014;62:1073–8.
57. Cheng XL, Li HX, Chen J, Wu P, Xue JH, Zhou ZY, et al. Bioactive diarylheptanoids from *Alpinia coriandriodora*. Nat Prod Bioprospect. 2021;11:63–72.
58. Liu SB, Zeng L, Xu QL, Chen YL, Lou T, Zhang SX, et al. Polycyclic phenol derivatives from the leaves of *Spermacoce latifolia* and their antibacterial and α-glucosidase inhibitory activity. Molecules. 2022;27:3334.

Publisher's Note